A Compliant and Redundantly Actuated 2-DOF 3RRR PKM: Best of Both Worlds?

Robin Cornelissen[1], Andreas Müller[2], and Ronald Aarts[1(✉)]

[1] Faculty of Engineering Technology, Structural Dynamics, Acoustics and Control, University of Twente, P.O. Box 217, 7500 AE Enschede, The Netherlands
R.J.Cornelissen@student.utwente.nl, R.G.K.M.Aarts@utwente.nl
[2] Institute of Robotics, Johannes Kepler University Linz, Altenbergerstraße 69, 4040 Linz, Austria
a.mueller@jku.at

Abstract. Due to their deterministic behaviour, compliant mechanisms are well-suited for high-precision applications. In this paper the benefits of redundant links and actuation are investigated in terms of increasing support stiffness and homogenising actuator loads.

The manipulator is modelled with lumped inertia properties of the links and non-linear relations for the joint stiffnesses. The lumped parameter model allows a fast system level performance optimisation of the joint geometry simultaneously exploiting joint pre-bending and preloading, where the stiffness matrices of all joints are computed numerically efficient with non-linear flexible beam elements.

This model is applied to optimise the design of a compliant and redundantly actuated 2-DOF 3RRR parallel kinematic manipulator. The improvement of support stiffness is demonstrated with an analysis of the first parasitic natural frequency. Balancing of the actuator torques is concluded from a potential energy analysis.

1 Introduction

In precision applications compliant mechanisms, or more precisely flexure-based mechanisms, are frequently used where the motion is enabled by elastic deformation of slender elements. Deterministic behaviour is ensured by the absence of friction, hysteresis and backlash. However, in spite of significant recent achievements in terms of the range of motion [6], it remains a challenge to maintain a high support stiffness, i.e. stiffness in directions in which the mechanism is not supposed to move, especially when the flexure joints in the mechanism undergo large deflections.

Redundantly actuated parallel kinematic manipulators (PKM) are researched to combine the advantages of PKM, i.e. the high stiffness, low inertia and large accelerations, with an improved handling of singularities and optimised actuator

A. Kecskeméthy and F. Geu Flores (Eds.): ECCOMAS 2019, COMPUTMETHODS 53, pp. 163–171, 2020.
https://doi.org/10.1007/978-3-030-23132-3_20

loading made possible by the redundancy [3,5]. In [4] the design of an experimental planar 2-DOF test setup with three actuators has been presented. The platform is well suited to evaluate models and control strategies.

The main goal of the present paper is to investigate whether the combination of compliant joints and redundant actuation can be exploited to further improve the dynamic properties of PKM, while circumventing the drawbacks of compliant joints. More specifically, the support stiffness from additional links is expected to reduce the decrease of this stiffness commonly observed at large joint angles. Furthermore, the redundant actuation offers a possibility to combine load balancing techniques with preloading of the compliant joints to balance the actuator effort, which is needed to position the end-effector (EE) at any position except for the equilibrium position, i.e. the centre of the workspace.

For this analysis the manipulator has to be modelled taking the non-linear stiffness of the joints into account. Such joint models are usually rather complicated and hence computationally too expensive when used to optimise the manipulator dynamic performance. For this reason many studies, including [6,7], investigate a single compliant joint. We propose to describe the complete manipulator with lumped inertia properties of the links and non-linear relations for the stiffness matrices of the joints. The lumped model allows a fast system level performance evaluation that is used to determine optimal joint orientation, pre-bending and preloading. The stiffness matrix of each joint depends on the joint geometry. It is computed throughout the full operating range of the joint where leaf springs are modelled with the non-linear flexible beam elements of the SPACAR software package [2]. Next piecewise linear interpolation is used to approximate all coefficients in this matrix as functions of the joint angle.

The main part of this paper are the analysis and optimisation methods for the support stiffness, Sect. 3, and actuator torques, Sect. 4. These are applied to the example manipulater introduced in Sect. 2. The results are presented and discussed in Sect. 5 with conclusions in Sect. 6.

2 Example Manipulator

The dynamic and kinetostatic models developed in the next sections will be demonstrated for a planar 2-DOF 3$\underline{\text{R}}$RR PKM equipped with compliant joints, Fig. 1(a). The three arms of the manipulator are similar but rotated 120° relative to each other. The shoulder joints and actuators are located at the vertices of an equilateral triangle, Fig. 1(b). This figure illustrates the basic geometric parameters like the total length L of each arm and the distance R of each actuator to the centre of the triangle. The workspace reachable by the EE is bounded by three circular arcs with radii L as indicated with the unshaded area in the figure. In order to reach all points within this workspace, the joints have to allow joint angles in some range. The ranges for the shoulder and elbow joints are indicated in the figure with the angles $\theta_{\text{s}}^{\text{r}}$ and $\theta_{\text{e}}^{\text{r}}$, respectively. These angles depend on the ratio L/R and the division of the total arm length L into the upper arm

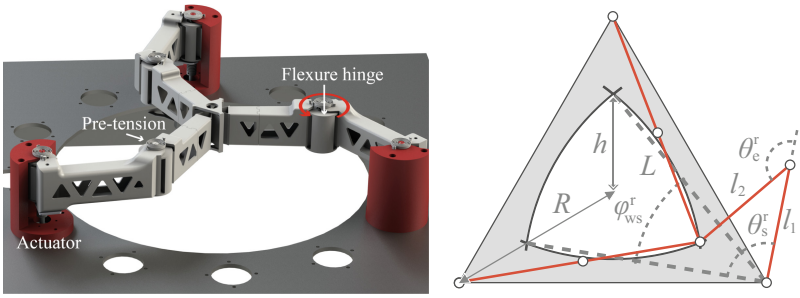

(a) Schematic manipulator overview. (b) Workspace.

Fig. 1. Planar 2-DOF 3RRR PKM similar to [4] except for the use of compliant joints, Fig. 2.

length l_1 and forearm length l_2. For the manipulator considered in this paper these dimensions are

$$R = 0.2305 \text{ m}, \quad L = 0.2536 \text{ m}, \quad l_1 = l_2 = L/2. \tag{1}$$

Then the joint angles ranges, with the lower and upper limit between brackets, are:

$$\theta^{r}_{s} = 50°(-17°...33°), \quad \theta^{r}_{e} = 83°(-49°...34°), \quad \theta^{r}_{w} = 50°(-22°...28°). \tag{2}$$

All compliant joints used in this example manipulator are butterfly joints, Fig. 2 [1]. For the shoulder joints this joint type is selected as it is known for its small pivot shift which makes it relatively easy to connect a common rotational

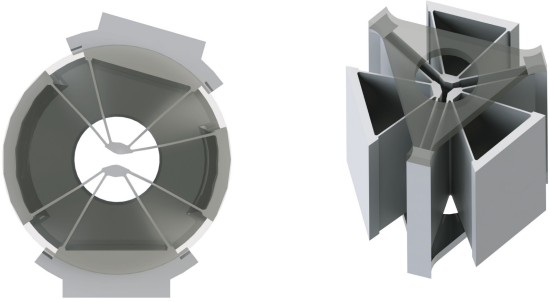

(a) Elbow joint (pre-bended). (b) Wrist joint.

Fig. 2. Two of the three compliant butterfly joint of the planar 2-DOF 3RRR PKM. The "intermediate" body that rigidly connects two or three connections between leaf springs are positioned on the top and bottom of the hinge and the top part is transparent in the images.

actuator to the upper arm. The elbow joints exhibit rather large rotation angles for which other joint types may be more favourable [6], but also a butterfly joint will be used to limit the overall complexity of the manipulator, Fig. 2(a). Finally, the wrist needs some special attention as it has to connect three links, Fig. 2(b). To maintain the symmetry as well as sufficient support stiffness, butterfly joints connect each forearm to an intermediate body. This extra body introduces an additional degree of freedom with a vibration mode with a relatively low frequency that has to be taken into account in the dynamic analysis of Sect. 3.

3 Support Stiffness Homogenisation

The support stiffness of compliant manipulators is often evaluated from the system's natural frequencies as in this way an implicit scaling of translational and rotational stifnesses is obtained. For a 2-DOF manipulator the first and second natural frequencies should be low as these are associated with the motion of the intended two degrees of freedom. The third natural frequency is the first parasitic frequency that should be as high as possible throughout the entire workspace. These natural frequencies can be computed with a detailed non-linear model of the full manipulator in which the EE position is varied in its entire workspace. For a design optimisation the evaluation of many alternative designs will be needed and such model would be too computationally intensive. Hence, a simplified lumped model is proposed.

This lumped parameter model should account for the mass properties of the rigid links and the stiffnesses of the joints. For the example manipulator of Sect. 2 seven rigid bodies can be identified, i.e. three upper arms, three forearms and the intermediate body connecting all forearms. Each body is characterised by its 6×6 mass matrix that is constant in a local frame connected to the body.

The links are connected to each other and the ground with nine joints in the shoulders, elbows and wrist. For each joint its full 6×6 stiffness matrix should be considered. For a specific joint with known dimensions this matrix can be evaluated numerically e.g. in the joint's pivot in the undeflected state. The non-linear flexible beam elements implemented in the SPACAR software package [2] have proven to be well-suited for efficient modelling of various compliant joint types [6,7]. Even when large deflections are considered three or four beam elements suffice for each leaf spring. Some known limitations arising from the beam model can be corrected like the torsional stiffening due to constrained warping in short and wide leaf springs [7]. With this model the stiffness matrix of each joint is computed throughout the full operating range of the joint and piecewise linear interpolation is used to approximate its coefficients as functions of the joint angle.

At system level all degrees of freedom of the rigid links are combined. In the example manipulator the seven links have 42 degrees of freedom in total. For a straightforward eigenvalue analysis it is proposed to define these independent coordinates in a coordinate frame located at the EE and aligned with the global coordinate frame. For the system level mass matrix the link mass matrices $\mathbf{M}_{\mathrm{upp}i}$,

$\mathbf{M}_{\mathrm{for}i}$, $\mathbf{M}_{\mathrm{int}}$ for upper arm i, forearm i and intermediate body respectively are combined to a block diagonal matrix $\mathbf{M}$. Similarly, the joint stiffness matrices are combined by adding the stiffness matrices $\mathbf{K}_{\mathrm{s}i}$, $\mathbf{K}_{\mathrm{e}i}$, $\mathbf{K}_{\mathrm{w}i}$ of shoulder i, elbow i and wrist i respectively,

$$\mathbf{K} = \begin{bmatrix} \mathbf{K}_{\mathrm{s1}} + \mathbf{K}_{\mathrm{e1}} & -\mathbf{K}_{\mathrm{e1}} & 0 & 0 & 0 & 0 & 0 \\ -\mathbf{K}_{\mathrm{e1}} & \mathbf{K}_{\mathrm{e1}} + \mathbf{K}_{\mathrm{w1}} & 0 & 0 & 0 & 0 & -\mathbf{K}_{\mathrm{w1}} \\ 0 & 0 & \mathbf{K}_{\mathrm{s2}} + \mathbf{K}_{\mathrm{e2}} & -\mathbf{K}_{\mathrm{e2}} & 0 & 0 & 0 \\ 0 & 0 & -\mathbf{K}_{\mathrm{e2}} & \mathbf{K}_{\mathrm{e2}} + \mathbf{K}_{\mathrm{w2}} & 0 & 0 & -\mathbf{K}_{\mathrm{w2}} \\ 0 & 0 & 0 & 0 & \mathbf{K}_{\mathrm{s3}} + \mathbf{K}_{\mathrm{e3}} & -\mathbf{K}_{\mathrm{e3}} & 0 \\ 0 & 0 & 0 & 0 & -\mathbf{K}_{\mathrm{e3}} & \mathbf{K}_{\mathrm{e3}} + \mathbf{K}_{\mathrm{w3}} & -\mathbf{K}_{\mathrm{w3}} \\ 0 & -\mathbf{K}_{\mathrm{w1}} & 0 & -\mathbf{K}_{\mathrm{w2}} & 0 & -\mathbf{K}_{\mathrm{w2}} & \mathbf{K}_{\mathrm{w123}} \end{bmatrix}, \tag{3}$$

where $\mathbf{K}_{\mathrm{w123}} = \mathbf{K}_{\mathrm{w1}} + \mathbf{K}_{\mathrm{w2}} + \mathbf{K}_{\mathrm{w3}}$. It should be noted that the link mass and joint stiffness matrices are initially computed in a local frame attached to the links' centre of mass or the joints' pivots, respectively. For each EE position the inverse kinematic solution for all links and joints can be found relatively easy. With these geometric data all link and joint matrices can be transformed to the EE frame with pre and post multiplication with adjoint matrices that reflect the involved sequence of translations and rotations.

Recall that for each joint the coefficients of the stiffness matrix are linearly interpolated as functions of the joint angle. In the transformation to the EE frame the joint orientations γ_{s} and γ_{e} of shoulder and elbow joints are design parameters. Additionally the shoulder and elbow joints can be manufactured with pre-bending angles β_{s} and β_{e}. These angles specify an offset between the joint angles at which the EE is in its equilibrium position and at which the joint is in the undeflected configuration, i.e. exhibits the largest support stiffness. In the computation of the actual joint stiffness, these pre-bending angles have to be added to the angles used in the linear interpolations.

4 Actuator Torque Balancing and Potential Energy

For the analysis of the support stiffness in the previous section, in particular the joint stiffnesses in the stiff directions play a role. The compliant directions are less relevant as the lowest natural frequencies are discarded. However, the actuator torques needed to position the EE depend on these joint stiffnesses and can be computed from a kinetostatic analysis. Each joint is described by a stiffness $k_{\mathrm{s}i}$, $k_{\mathrm{e}i}$ or $k_{\mathrm{w}i}$ in the driving direction, which is the lower right coefficient in the respective stiffness matrix of the previous section and is weakly dependent on the joint angle. Furthermore, for the shoulder and wrist joints pretension angles α_{s} or α_{e} are taken into account. This pretension angle is defined as the joint angle at which the joint is undeformed and hence no joint torque arises.

For any EE position the motor torques τ_i $(i = 1, 2, 3)$ acting on the shoulder joints needed to keep the system statically balanced can be determined from equilibrium equations that can be derived for all links. As the manipulator is redundantly actuated, there is no unique solution for the actuator torques.

The null space solution is used to compute the actuator torques that minimise the 2-norm of the vector $\boldsymbol{\tau}$ with the three actuator torques τ_i [4]. It appears that this actuator norm $||\boldsymbol{\tau}||$ scales proportionally to the variation of the potential energy in the compliant joints throughout the workspace, which is relatively easy to evaluate in order to optimise the joint pretension angles α_s and α_e.

5 Results

The analysis methods outlined in the previous sections will now be applied for the design of the example manipulator proposed in Sect. 2. For high performance metal links and joints would be preferred, but for a cost-effective first prototype it is chosen to use 3D printed parts made by Selective Laser Sintering (SLS) of Nylone (PA2200). Typical material properties are its Young's modulus $E = 1.7$ GPa and density $\rho = 930$ kg/m^3. Preloading of the joints is not possible with this material as creep will result in rather quick unloading. Hence an alternative solution for preloading should be applied like low-stiffness preloaded (metal) springs positioned parallel to the joints, as can be recognised in Fig. 1(a).

Homogenised Support Stiffness. As outlined in Sect. 2 it was chosen to use butterfly hinges for all joints in the example manipulator. Butterfly hinges have an extra internal degree of freedom due to rotation of an intermediate body which may show a relatively low frequent vibration mode. This motion can be constrained [1] when its frequency appears to be too low. As was also pointed out in Sect. 2, the EE has an intermediate body as well for which the same consideration applies. For the considered manipulator it appeared that lightweight intermediate bodies can be used, such that the natural frequencies of the internal modes were higher than some other parasitic mode and hence no precautions had to be taken to constrain these modes.

Figure 3 illustrates some steps in the optimisation procedure of which Table 1 summarises some geometric parameters. In Fig. 3(a) the variation of the support stiffness throughout the EE workspace is evaluated in terms of the first natural frequency for some initial design. For butterfly joints the reduction of the support stiffness is relatively small as is shown in Fig. 4. Nevertheless the first parasitic natural frequency varies more that a factor 2 throughout the workspace.

Table 1. Geometric parameters of optimised joints. The vertical dimension of all hinges is 40 mm. The thickness of all leaf springs is 0.4 mm. The table shows the other in-plane dimensions.

	Shoulder		Elbow		Wrist
	Height [mm]	Width [mm]	Height [mm]	Width [mm]	Height [mm]
Individual hinge optimisation	27.4	12.2	25.7	10.1	17.9
Full optimisation	20.2	19.8	29.4	17.8	18.2

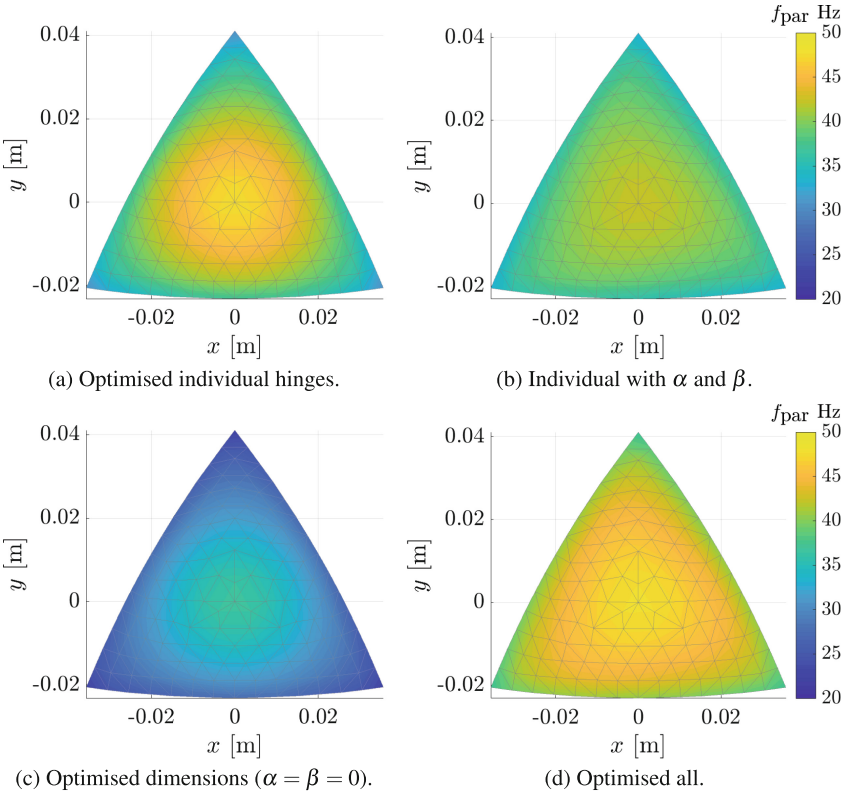

(a) Optimised individual hinges.

(b) Individual with α and β.

(c) Optimised dimensions ($\alpha = \beta = 0$).

(d) Optimised all.

Fig. 3. Optimising the support stiffness, evaluated with the first parasitic natural frequency.

With an optimal pre-bending and joint orientation this variation can be reduced as shown in Fig. 3(b), although the primary optimisation goal is increase of the lowest frequency near the corners. Probably the redundant arm also offers additional homogenisation of the stiffness.

A further improvement is possible by optimising the joint parameters, Fig. 3(c), and finally combining all optimisation efforts, Fig. 3(d). In the final result, not only the lowest parasitic natural frequency has been increased, but also its largest value near equilibrium is large again although this was not an optimisation goal.

Balanced Actuator Torques. In the design so far the actuator torques are not considered. To illustrate the actuator torque balancing, Fig. 5 shows the potential energy E stored in the compliant joints relative to the equilibrium configuration. The figure shows the steep increase in energy storage towards the extreme edges of the workspace without pretensioned compliant joints ($\alpha_{\text{s}} = \alpha_{\text{e}} = 0°$). With pretension a significant reduction of the potential energy is possible as is demonstrated in the figure with $\alpha_{\text{s}} = 42°$, $\alpha_{\text{e}} = -50°$. The torque

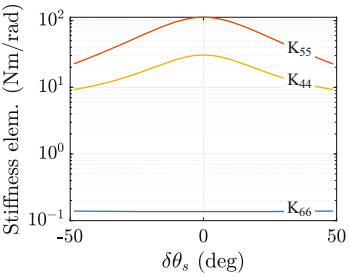

Fig. 4. Joint stiffness of the butterfly shoulder hinge in driving (K_{66}) and two support (K_{44}, K_{55}) directions.

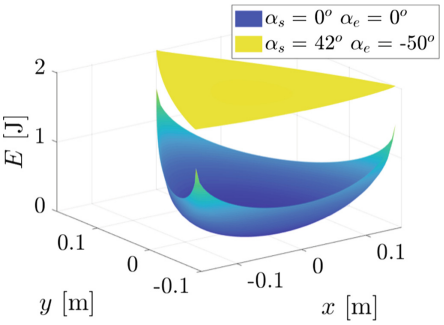

Fig. 5. Balanced potential energy storage illustrating the balancing of the driving torque.

norm $||\boldsymbol{\tau}||$ scales similarly, hence a reduction of the driving torques with more than an order of magnitude is achieved by this balancing.

6 Conclusion

In this paper we propose an analysis method that enables a system level optimisation of a parallel kinematic manipulator with redundant actuation and compliant (or flexure) joints. The goal of the optimisation is to combine the redundancy with preloading and pre-bending of the joints to obtain a high support stiffness throughout the workspace and to reduce the actuator torques. The approximate model used in this optimisation combines lumped mass properties of the rigid links with non-linear stiffness matrices of the joints computed as functions of the joint angles.

The method is applied to the design of a planar 2-DOF 3RRR parallel manipulator. It appears that orientation and pre-bending of the compliant joints can be optimised to avoid a significant decrease of the support stiffness and preloading helps to lower the required actuator torques. The proposed design has been manufactured with 3D printing to experimentally verify the expected dynamic behaviour, as will be published in the future.

References

1. Henein, S., Spanoudakis, P., Droz, S., Myklebust, L.I., Onillo, E.: Flexure pivot for aerospace mechanisms. In: Proceedings of the 10th European Space Mechanisms and Tribology Symposium, San Sebastian, Spain (2003)
2. Jonker, J.B., Meijaard, J.P.: SPACAR - computer program for dynamic analysis of flexible spatial mechanisms and manipulators. In: Schiehlen, W. (ed.) Multibody Systems Handbook, pp. 123–143. Springer, Heidelberg (1990)

3. Kock, S., Schumacher, W.: A parallel x-y manipulator with actuation redundancy for high-speed and active-stiffness applications. In: Proceedings of the 1998 IEEE International Conference on Robotics and Automation, Leuven Belgium, pp. 2295–2300 (1998)
4. Krajoski, K., Müller, A., Gattringer, H., Jörgl, M.: Design, modeling and control of an experimental redundantly actuated parallel platform. In: Niel, K., Roth, P.M. (eds.) Proceedings of the OAGM&ARW Joint Workshop 2016 "Computer Vision and Robotics", University of Applied Sciences Upper Austria, Wels Campus, pp. 209–216 (2016)
5. Müller, A., Hufnagel, T.: Model-based control of redundantly actuated parallel manipulators in redundant coordinates. Robot. Auton. Syst. **60**(4), 563–571 (2012)
6. Naves, M., Brouwer, D.M., Aarts, R.G.K.M.: Building block-based spatial topology synthesis method for large-stroke flexure hinges. J. Mech. Robot. **9**(4), 041006 (2017). 9 pages
7. Wiersma, D.H., Boer, S.E., Aarts, R.G.K.M., Brouwer, D.M.: Design and performance optimization of large stroke spatial flexures. J. Comput. Nonlinear Dyn. **9**(1), 011016 (2013). 10 pages